Correlation of RF Signals During Angular Compounding

Quan Chen, *Student Member, IEEE*, Anthony L. Gerig, *Member, IEEE*, Udomchai Techavipoo, *Member, IEEE*, James A. Zagzebski, *Associate Member, IEEE*, and Tomy Varghese, *Senior Member, IEEE*

***Abstract*—A theoretical analysis of the correlation between radio-frequency (RF) echo signal data acquired from the same location but at different angles is presented. The accuracy of the theoretical results is verified with computer simulations. Refinements to previous analyses of the correlation of RF signals originating from the same spatial location at different angular positions are made. We extend the analysis to study correlation of RF signals coming from different spatial locations and eventually correlation of RF signal segments that intersect at the same spatial location. The theory predicts a faster decorrelation with a change in the insonification angle for longer RF echo signal segments. As the RF signal segment becomes shorter, the decorrelation rate with angle is slower and approaches the limit corresponding to the correlation of RF signals originating from the same spatial location. Theoretical results provide a clear understanding of angular compounding techniques used to improve the signal-to-noise ratio in ultrasonic parametric imaging and in elastography.**

I. Introduction

Pulse-echo ultrasound images, as well as many forms of parametric ultrasound images [1]–[13], are subject to statistical fluctuations caused by the random locations of scatterers that contribute to the instantaneous backscattered echo signal. When the scatterers are densely distributed, radio-frequency (RF) echo signals obey Gaussian statistics, while the envelope of the signal follows a Rayleigh distribution [14], [15]. Thus, the ratio of the mean echo signal at any point to its standard deviation is fixed at 1.91 for sonograms. The resultant speckle decreases contrast detectability on B-mode images and leads to significant uncertainties of parameters derived for quantitative images [16].

To partially overcome this limitation, researchers have proposed the use of spatial and frequency compounding in which data for a particular spatial location are averaged from different look directions or different frequencies within the transducer bandwidth [17]–[19]. Some B-mode equipment manufacturers have adopted spatial compounding for use with linear and curvilinear array systems, and this appears to improve contrast detectability in many instances [20], [21]. Our group has recently introduced angular spatial compounding techniques for the production of parametric images of attenuation, scatterer size, and strain [16], [22]–[25]. Angular spatial compounding can significantly improve the statistical properties of these images, affecting the tradeoff between spatial resolution and image signal-to-noise ratios (SNR). Following the analysis by O'Donnell [9], performing angular compounding by translating the aperture by an amount equal to the aperture size improves the SNR of B-mode images by a factor of 1.67 (2.8 independent views).

Spatial compounding is most effective when signals to be averaged are uncorrelated. Numerous studies have been done to investigate spatial correlations in speckle fluctuations in medical ultrasonic images [14], [15], [26]–[29], and the salient results are summarized by Wagner *et al.* [15]. These prior approaches use an impulse response, or point-spread-function (PSF), to describe the ultrasound system and subsequent modeling of the ultrasound signals. Other investigators start from an accurate representation of the ultrasound system with equations formulating field calculation [30], [31]. However, various approximations are then utilized to obtain simplified representations for the signal correlation, basically reverting back to the PSF representation. Most of these derivations lead to the same expression for the signal decorrelation during spatial compounding as used by Wagner *et al.* The K-space representation proposed by Walker and Trahey [30] offers insight into the sources of ultrasound signal correlation. However, it can be viewed as the Fourier transformation of the time-domain PSF approach. Walker and Trahey [30] compare their results with those of Wagner *et al.* to prove the validity of their theory. Zemp *et al.* [31] apply an impulse response approach, expressing the impulse response in an analytical form, with ultrasound field calculations taken into account to model ultrasound signals. Their primary contribution is to define a function called spatial-sensitivity-function (SSF) and point out its relationship to the PSF. However, applying their method to this problem requires a numerical calculation of the ultrasound field rather than yielding an analytical expression for the problem.

The previous studies were directed mainly toward B-mode image compounding, where the theories developed were for the study of correlations between echo signals

Manuscript received November 11, 2003; accepted October 22, 2004. This research was supported in part by NIH grants T32CA09206, R21EB002722, R21EB003853-01, and R21EB003853.

The authors are with the Department of Medical Physics, The University of Wisconsin-Madison, Madison, WI-53706 (e-mail: jazagzeb@wisc.edu).

U. Techavipoo and T. Varghese are also with the Department of Electrical and Computer Engineering and the Department of Biomedical Engineering, respectively, at The University of Wisconsin-Madison, Madison, WI 53706.

acquired from the same spatial location but different insonification angles. In parametric imaging of scatterer size [4], [16], integrated backscatter [12], [13], or spectral slope [32], the displayed data at each spatial location are estimated from a segment of RF echo data representing the region around it. When viewed at another angle, only the signal at the location where two RF lines intersect follows theories applicable to B-mode compounding. Since other sections of the RF data segment undergo greater decorrelation, previous theoretical results do not provide a complete solution. Therefore, a theory is needed to calculate the correlation of RF data segments at different insonification angles applicable for parametric image compounding, and this is the topic of this paper.

This paper is organized as follows. We first revisit the approach used by Wagner *et al.* [15] to derive the correlation between ultrasound echo signals that arise from points where angled beam lines intersect. We then establish general equations that describe the correlation between signals obtained with intersecting beams, accounting for contributions to each signal from locations away from the intersection point. With this result, we obtain the correlation between RF echo signal segments for different insonification angles, which is the main contribution of this paper. The correlation between signal segments from parallel beam lines also emerges with our general approach. Differences between our expressions and those of Wagner *et al.* [15] are discussed. Finally, simulation studies are presented that verify the theoretical expressions, and these demonstrate close correspondence between decorrelation vs. beam angle for simulated data and from theoretical curves. Factors that affect the correlation vs. beam angle curve are also explained with the help of simulations.

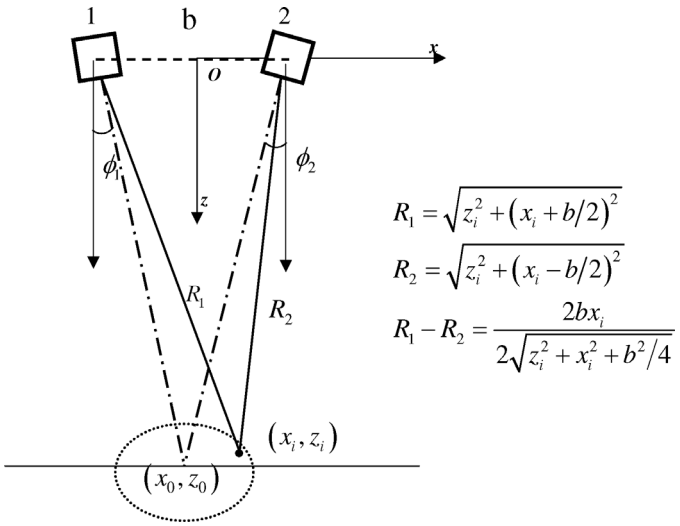

Fig. 1. Schematic illustration of a transducer insonifying scatterers at position (x_0, z_0) from transducer location 1. The transducer is then translated to location 2 and rotated or steered to view the same position.

II. Theory

A. Correlation Between Signals from the Same Spatial Location

As illustrated in Fig. 1, a transducer insonifies and interrogates a region in its focal zone containing scattering particles uniformly distributed over the scattering volume in random positions. The cumulative signal amplitude s at transducer position 1 from scatterers in the medium can be written as:

$$s_1 = \sum_i |T_i|\,|p_{1,i}| \exp(j\vartheta_i), \tag{1}$$

where subscript i refers to an individual scatterer, $|T_i|$ represents the magnitude of the scattering amplitude from the ith particle, $|p_{1,i}|$ is the magnitude of the pulse-echo point spread function from the scatterer at position i received by transducer 1, and $\exp(j\vartheta_i)$ represents the combined phase of $|T_i|$ and $|p_{1,i}|$. Now the transducer is translated a distance b and rotated or steered to insonify the same scattering region as location 1. We establish our coordinates by setting the transducer shift vector as the x axis, the vector perpendicular to the shift direction as the z axis, and the midpoint of the shift as the origin. The point where the axes of both beam lines intersect has coordinates (x_0, z_0). The angle between the beam axis at transducer position 1 and the z axis is ϕ_1, and the angle between the axis at position 2 and the z axis is ϕ_2. For the signal received from the ith scatterer at (x_i, z_i), a phase difference $4\pi b x_i / r_i \lambda_0$ exists between signals for the two transducer positions, where λ_0 is the wavelength at the center frequency, and $r_i = \sqrt{x_i^2 + z_i^2 + b^2/4}$ can be seen as the average distance from the scatterer to the transducer surface for the two locations. The factor of two in the phase accounts for the two-way pulse-echo path. The cumulative signal strength at position 2 can then be written as:

$$s_2 = \sum_i |T_i\,|p_{2,i}|| \exp(j\vartheta_i) \exp(4\pi j b x_i / r_i \lambda_0). \tag{2}$$

The cross-correlation between the signals acquired at transducer positions 1 and 2 is given by:

$$\langle s_1 s_2^* \rangle = \sum_i |T_i|^2 |p_{1,i}|\,|p_{2,i}| \exp(4\pi j b x_i / r_i \lambda_0). \tag{3}$$

We now invoke separability of the point spread function to divide it into lateral and range (axial) components. For the ith scatterer at (x_i, z_i), the lateral distances to the beam axis for transducer positions 1 and 2 are, respectively,

$$l'_n = (x_i - x_0)\cos\phi_n - (z_i - z_0)\sin\phi_n, \quad (n = 1, 2). \tag{4}$$

Similarly, the axial distances to the intersection point (x_0, z_0) are:

$$l''_n = (x_i - x_0)\sin\phi_n + (z_i - z_0)\cos\phi_n, \quad (n = 1, 2). \tag{5}$$

Eq. (3) becomes:

$$\langle s_1 s_2^* \rangle = \sum_i |T_i|^2 |p'(l_1')\|p''(l_i'')\|p'(l_2')\|p''(l_2'')| \times \exp(4\pi j b x_i / r_i \lambda_0), \quad (6)$$

where p' represents the lateral beam spread function, and p'' represents the axial spread function. For a rectangular aperture, for example, the lateral point spread function at the focus or in the far-field can be written as:

$$p'(x) = \sin^2(\pi f_0 x)/(\pi f_0 x)^2, \quad (7)$$

where $f_0 = D'/r\lambda_0$, D' is the effective transducer aperture, and r is the focal distance, $r = z_0/\cos\phi$.

If we assume that the ultrasound pulse transmitted by the transducer has a Gaussian envelope with characteristic width σ_z, then p'' can be expressed as:

$$p''(z) = \exp(-z^2/2\sigma_z^2). \quad (8)$$

Going to a continuous representation, x_i and z_i become x and z, and the summation in (6) becomes a 2-D integral about x and z. Thus,

$$\langle s_1 s_2^* \rangle = B'' \iint |p'(l_1')\|p''(l_1'')\|p'(l_2')\|p''(l_2'')| \times \exp(4\pi j b x / r\lambda_0) dx dz, \quad (9)$$

where

$$l_n' = (x - x_0)\cos\phi_n - (z - z_0)\sin\phi_n, \quad (n = 1, 2) \quad (10)$$

$$l_n'' = (x - x_0)\sin\phi_n + (z - z_0)\cos\phi_n, \quad (n = 1, 2) \quad (11)$$

$$r = \sqrt{x^2 + z^2 + b^2/4}, \quad (12)$$

and B'' is a normalization factor. An analytical closed-form solution for (9) is difficult to obtain. Thus, it is necessary to either resort to numerical solutions or apply approximations to simplify the expression.

Let us compare this result with that of previous authors. For the same geometrical arrangement, the expression of Wagner *et al.* [15] (using our notation) for the echo-signal cross-correlation can be written as:

$$\langle s_1 s_2^* \rangle = B'' \int |p'(x)|^2 \exp(4\pi j b x / z_0 \lambda_0) dx. \quad (13)$$

Eq. (13) follows the notation of a Fourier transformation (FT). The correlation function is therefore an FT of the square of the PSF:

$$\rho = \left[FT\left\{ |p'(x)|^2 \right\} \right]_{f = 2b/\lambda_0 z_0}. \quad (14)$$

For a rectangle aperture, this is a convolution of two triangular functions. This convolution was calculated analytically by O'Donnell and Silverstein [29] via the contour integral approach. The solution is given by:

$$\rho(x) = \begin{cases} 1 - 6x^2 + 6x^3 & x \le 1/2 \\ 2(1-x)^3 & 1 \ge x > 1/2, , \\ 0 & x \ge 1 \end{cases} \quad (15)$$

where x is the fractional displacement of the aperture, $x = b/D'$. Note that this equation implies that the angular decorrelation of signals arising from the intersection of two beams is independent of the insonification frequency. Although the beam width varies with frequency and would affect the volume of insonified scatterers, the relative phase of echo signals from individual scatterers also varies with frequency. Thus, it would appear that the two effects cancel, leaving the signal decorrelation a function of the aperture size only. We will show later in this paper that this behavior does not exist for angular decorrelation analysis for extended RF signal segments, however.

Wagner *et al.* [15] separate the PSF into lateral and range components, as $|p_i| = |p'(x)\|p''(z)|$. Implicit in this decomposition is the assumption that the tilt angle of the transducers can be neglected, *i.e.*, $\phi_{1,2} = 0$ in (4) and (5).

In (9), the phase term $\exp(4\pi j b x / r\lambda_0)$ contains a variable r, which is a function of x and z. Since only scatterers close to the intersection point of the beams contribute to the signal, we can approximate the phase term as $\exp(4\pi j b x / z_0 \lambda_0)$. We can then perform the integration in the lateral and range direction separately as in the Wagner *et al.* paper [15] and obtain the expression in (13)–(15).

B. Correlation Between Signals Arriving from Different Spatial Locations

The analysis described above applies to only one type of B-mode compounding, where signals from the same spatial location viewed from different angles are compounded. However, if we simply translate the transducer without tilting or steering to insonify the same location, where we are interested in the correlation of adjacent parallel beam lines, the derivation in Section II-A will not apply. Also, in parametric imaging modalities, such as scatterer size imaging [4], [5], [12], [13], [16], attenuation coefficient imaging [7], [12], [13], and elastography [10], parameters are estimated using gated segments of the RF signal. When we perform angular compounding in these imaging modalities, we must be aware that the signal decorrelation will arise not only from different insonification angles but also from different targets being interrogated when the gated region extends beyond the center of rotation.

To derive an expression that takes into consideration different target locations, we use the setup illustrated in Fig. 2. Two transducers separated by a distance b scan different locations separated by distance a. The cross-correlation between signals from transducer 1 and transducer 2 can be written as:

$$\langle s_1 s_2^* \rangle = B'' \iint |p'(l_1')\|p''(l_1'')\|p'(l_2')\|p''(l_2'')| \times \exp(4\pi j b x / r\lambda_0) dx dz, \quad (16)$$

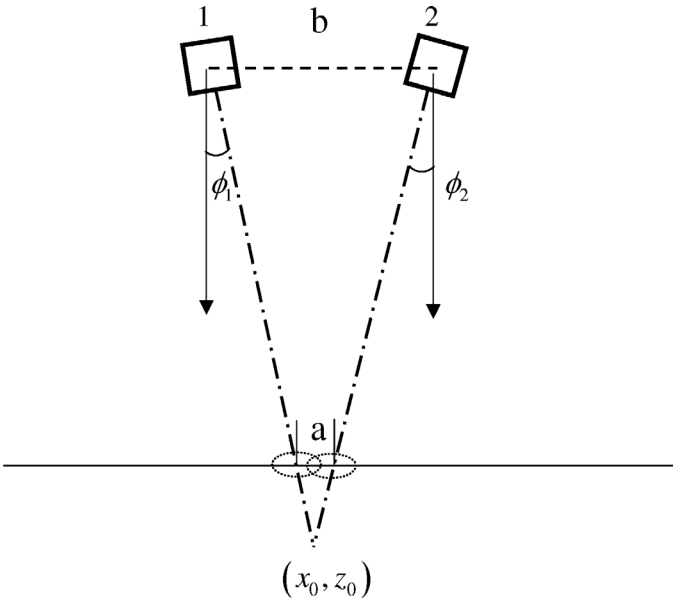

Fig. 2. Schematic illustration of a transducer translated a distance b and then rotated or steered to view the same position (x_0, z_0). Here signals arising from scatterers at various depths near the beam intersection point are considered. The origins of the signals are separated by a distance a.

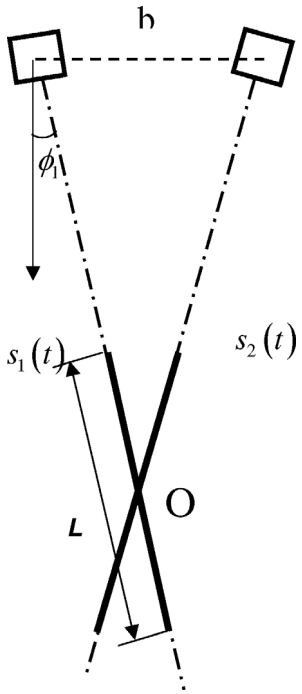

Fig. 3. Schematic illustration of the gated RF data segment acquired as a transducer is translated and rotated or steered to view the same position O. The thick line represents the gating window for the RF segment with length L. The RF segments acquired are represented as $s_1(t)$ and $s_2(t)$.

which is the same as (9). However, the lateral and axial distances now become:

$$l'_{1,2} = (x \pm a/2)\cos\phi_{1,2} - (z - z_0)\sin\phi_{1,2} \text{ and} \tag{17}$$

$$l''_{1,2} = (x \pm a/2)\sin\phi_{1,2} + (z - z_0)\cos\phi_{1,2}. \tag{18}$$

If we adopt the same approximation used for (14) and (15), we obtain:

$$\rho(a,b) = \left[FT\left\{|p'(x - a/2)\|p'(x + a/2)|\right\}\right]_{f=2b/\lambda_0 z_0}. \tag{19}$$

The above expression is the generalized cross-correlation function that takes into consideration different insonification angles as well as different scatterer locations. Note that unlike (14), numerical integration is required to obtain the exact form of the cross-correlation function from (19).

C. Correlation of RF Signal Segments that Intersect at the Same Spatial Location

In the case of parametric imaging, gated segments of the echo signal are applied. The tissue parameter at location O is estimated from RF segments illustrated with thick lines, as shown in Fig. 3. The RF signal received by transducer 1 is $s_1(t)$, and the RF signal received by transducer 2 is $s_2(t)$. A segment is selected using a window, for example, a rectangular window or a Hanning window. Normally, the same window is used to select both segments. The window function will modulate the signal intensity in the segment selected. Attenuation and focusing effects will also affect the signal intensity, and this will weigh the contribution of each scatterer to the correlation between angled RF signal segments. These effects can be included in the $w(t)$ term so that the intensity of $s(t)$ can be taken as constant with depth. Thus, the cross-correlation between two gated RF signal segments acquired at different insonification angles can be written as:

$$\rho_{1,2} = \frac{\left\langle \sum_{t=t1}^{t2} w^2(t) s_1(t) s_2^*(t) \right\rangle}{\left[\left\langle \sum_{t=t1}^{t2} w^2(t) s_1(t) s_1^*(t) \right\rangle \left\langle \sum_{t=t1}^{t2} w^2(t) s_2(t) s_2^*(t) \right\rangle \right]^{1/2}}. \tag{20}$$

The overall signal intensity viewed at different angles should be the same, provided the distance between the transducer and the sample volume remains constant and the change in beam width due to the changing aperture projection at different angles can be neglected. The denominator in (20), therefore, becomes:

$$\left\langle \sum_{t=t1}^{t2} w^2(t) s(t) s^*(t) \right\rangle. \tag{21}$$

The ensemble average operator can be moved inside the summation. As mentioned above, the signal intensity variations due to attenuation and focusing effects are included

in the $w(t)$ term so that the intensity of $s(t)$ is constant with depth. Eq. (21) becomes

$$\sum_{t=t1}^{t2} \left\langle w^2(t)s(t)s^*(t)\right\rangle = \overline{I} \cdot \sum_{t=t1}^{t2} w^2(t), \tag{22}$$

where $\overline{I} = \langle s \cdot s^* \rangle$ is the mean signal intensity.

Replacing the summation with an integral, (20) becomes:

$$\begin{aligned}\rho_{1,2}(2\phi_1) &= \frac{\int_{t_1}^{t_2} w^2(t)\left\langle s_1(t)s_2^*(t)\right\rangle / \overline{I} dt}{\int_{t1}^{t2} w^2(t)dt} \\ &= \frac{\int_{-L/2}^{L/2} w^2(\xi)\rho(2\xi\sin\phi_1, 2z_0\sin\phi_1)d\xi}{\int_{-L/2}^{L/2} w^2(\xi)d\xi},\end{aligned} \tag{23}$$

where L is the length of the RF segment, and the ρ inside the integral is the correlation of signals resulting from different locations and from different insonification angles, respectively. It can be either the numerical result of (16), or its approximated version (19). ξ is the distance from points in the volume giving rise to the RF segment to the rotation center, and z_0 is the distance from the line separating the transducers to the rotation center. $2\xi\sin\phi_1$ and $2z_0\sin\phi_1$ are terms corresponding to a and b in (19), respectively.

D. Correlation of Two Parallel RF Echo Signal Segments

Eq. (19) can also be used to calculate the correlation between signals acquired from two parallel beam lines in the same image. Under this circumstance, we have $a = b$. The correlation between signals from two beam lines acquired from an aperture separated a distance b, as in linear array imaging is:

$$\begin{aligned}\rho(b) &= \left[FT\left\{|p'(x-b/2)\|p'(x+b/2)|\right\}\right]_{f=2b/\lambda_0 z_0} \\ &= \int |p'(b-x)\|p'(b+x)|\exp(4\pi jbx/z_0\lambda_0)dx.\end{aligned} \tag{24}$$

This form is slightly different from the one in Wagner's paper [15] since he assumed that the ultrasound image is formed by the convolution of scatterers with the system PSF, and he neglects any differences in signal phase when viewed from two different angular positions.

However, we have to point out here that our formula does not produce results that are significantly different from the expression in Wagner's paper [15] when using transducer and medium parameters applicable to medical ultrasound. This is probably due to the fact that the phase term changes slowly compared to the PSF term under these imaging conditions. However, (24) is the more complete form of the expression.

III. Simulations

Computer simulations were used to verify the validity of the theoretical expressions derived in this paper. We generated simulated RF signals and compared the cross-correlation results obtained at different angular positions with theory. The simulations were performed by convolving random scatterers with a PSF calculated with a field calculation code described previously [33]. For the present study, we modeled a linear array consisting of elements of size 0.15 mm by 10 mm, with a center-to-center distance of 0.2 mm. A Gaussian-shaped pulse with a center frequency of 5 MHz and a -6 dB bandwidth of 50% was used as the incident pulse. We set both the transmit and receive focuses at 30 mm. The aperture used was 15 mm so that the F-number was 2. The pulse-echo PSF was calculated with the frequency-domain algorithm [33]. For the purpose of these simulations, the same PSF was applied throughout the signal segment, which facilitated the integration in (23) for comparison. Note that this simulation approach does not correspond to the actual ultrasound imaging process where a fixed transmit focus and a dynamic receive focus are used. Under those conditions, the PSF would be a sinc function for most depths, except near the transmit focus where it would be a sinc-square function. Also, the actual imaging process will involve a dynamic aperture. Although our simulation program [33] can successfully simulate all of these features, for the purpose of this paper where we are interested only in verifying the theoretical equations, a simplified model is sufficient as long as we use the same assumption in both the theory and the simulation.

A uniform phantom was simulated by modeling a random distribution of 50 μm polystyrene beads in a medium that has a speed of sound of 1540 m/s. The attenuation of the phantom was set at zero so that the signal intensity would be uniform for all depths. The scatterer number density was set at 9.7 per cubic millimeter, which is more than sufficient for a Rayleigh distribution of the echo signal envelope since Rayleigh statistics apply for approximately 10 or more scatterers per resolution cell [15]. The frequency dependence of the backscatter coefficient of the 50-μm polystyrene beads was calculated using Faran's theory [34] and was incorporated into the PSF calculation. The modeled phantom dimensions were 60 mm (width) by 50 mm (height) by 10 mm (thickness). After modeling the echo signals for a single pulse-echo sequence, the phantom model was rotated around its center to obtain RF signals at different insonification angles. This rotation operation maintained the locations of all scatterers relative to each other, so changes in phase and amplitude of returning echoes during the rotation are accurately represented. The rotation angle was varied from 0 to 90 degrees, with an angular increment of 0.5 degrees. In an actual linear array, beam steering cannot be approximated by simply rotating the same beam because the effective aperture may change slightly in the beam-steering process. However, as discussed in the previous paragraphs, the approach is suf-

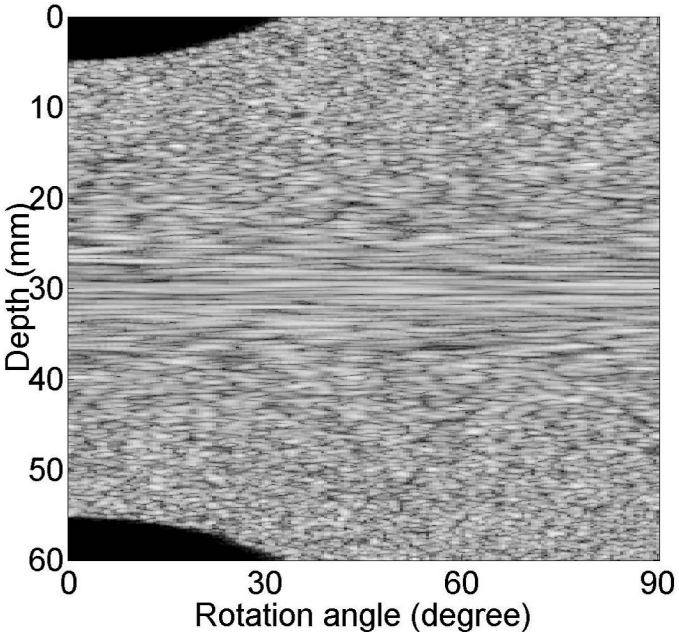

Fig. 4. B-mode-like display of echoes from along a single beam line passing through the rotation center of a phantom as the phantom is rotated over a 90-degree angle. The image would be the same if a transducer were rotated around the phantom to view the center of the phantom. The farther away from the rotation center, the faster the texture varies as the phantom is rotated.

ficient to verify the theoretical derivation presented in this paper.

IV. Results

The RF signals obtained at each insonification angle were envelope-detected and log-compressed. They were then formatted to form a B-mode-like image, and this is shown in Fig. 4. This image is obtained using only the central beam line for each acquisition angle. Thus, the x-axis is the rotation angle, and each vertical line represents the B-mode signals viewed for the central line at that angle. The difference in texture at different depths is due to the difference in relative lateral displacements of reflectors during rotation, from the beam's eye view. It is obvious from the image that echo signals arriving from points farther away from the rotation center decorrelate at a faster rate than signals at points near the rotation center.

We ran simulation experiments using various lengths of RF segments centered at the rotation center, and then computed the normalized cross-correlation function to obtain correlation coefficient estimates. A rectangular window was used to segment the RF segment. Since we avoided signal intensity variations due to attenuation and focusing effects in our simulations, the window function $w(t) \equiv 1$. A correlation coefficient curve obtained using 0.39-cm-long simulated RF segments is plotted in Fig. 5(a). Each data point represents the average of cross-correlation coefficients from a number of RF segment pairs corresponding to the same insonification angle difference. For example, the data point at 1.5 degrees represents the average of all the cross-correlation coefficient estimates from RF segment pairs obtained at 0 degree and 1.5 degrees, 1.5 degrees and 3 degrees, etc. The data points at larger angular shifts are derived from fewer averaged correlation coefficient data points and are, therefore, less reliable. The error bars span plus and minus two standard deviations from the mean cross-correlation coefficient. The theoretical prediction, obtained by numerically calculating (23), is plotted as a dashed line. The correlation coefficient curves obtained using simulated RF data segment lengths of 0.78 cm, 1.57 cm, and 3.14 cm are plotted in Fig. 5(b), (c), and (d), respectively. Although these segment lengths are arbitrary, they demonstrate that there is excellent agreement between simulation results and theoretical predictions at all RF segment lengths.

V. Discussion

In angular B-mode compounding, where B-mode images are acquired from different view angles and superimposed, the signals to be compounded arrive from approximately the same spatial location, ensuring no loss in spatial resolution providing the aperture is not decreased. Decorrelation is incurred among the signals from different view angles because the relative positions of the scatterers within the resolution cell change as the beam rotates.

Compound echo data acquisition and display can also reduce the noise in parametric ultrasound data, but at the expense of additional processing time required for parameter estimations along angular directions. The most efficient use of processing time would occur if the data acquired from different angular directions were statistically independent. Since a significant correlation exists between echo signals acquired from adjacent beam lines or small angular increments on an ultrasound scanner, it is useful to understand how these system factors affect the correlation between signals.

This paper extends the work of Wagner *et al.* [15] by considering the decorrelation of signals arising from extended data segments, as are often used in parameter estimations. The decorrelation of RF segments with beam angle depends on the segment length, as shown in Fig. 5. Theoretical predictions of the normalized correlation coefficient values for different lengths of RF signal segments are shown in Fig. 6. Here the decorrelation of signals that arise from the point where the beams intersect is indicated by the "0 cm" line. The functional dependence exhibited by the 0-cm line is predicted by previous theory [15], [29]. As expected, when points farther away from the rotation center are included in the gated data segment, the signal decorrelates with angle at a faster rate. With shorter RF segments, the cross-correlation curve slowly approaches the "zero-length" limit, predicted by (15). If the data window used in parametric imaging is in the millimeter range, we could use (15) for estimating the degree of correlation with shifts in the insonification angle.

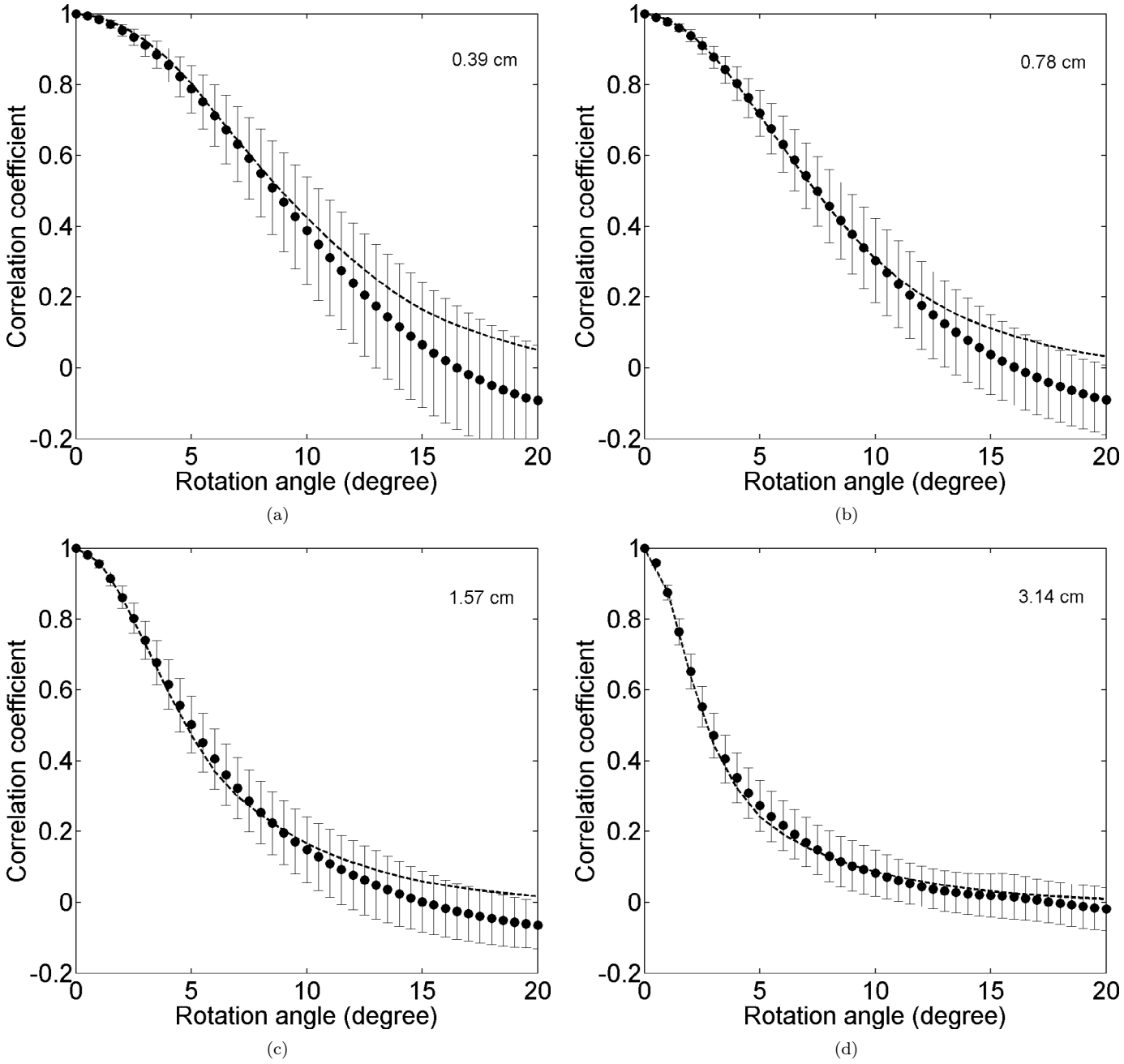

Fig. 5. Comparison between theoretical prediction and simulation result of the correlation coefficient of RF segments acquired at different insonification angles. Results are shown for RF segment lengths of (a) 3.14 cm, (b) 1.57 cm, (c) 0.78 cm, and (d) 0.39 cm. The dashed line denotes theory, while the solid circles and error bars are calculated from simulations.

As the length of the RF segment increases, the scatterers included in the gated segment are farther from the rotation center. Then, as the insonification angle changes, new scattering sources are interrogated, especially for depths near the edges of the gated region, causing the signal to decorrelate faster. This increase in decorrelation is due primarily to the ultrasound beam interrogating different spatial regions, which is similar to the decorrelation that would occur if data from adjacent beam lines on an ultrasound image were averaged. Therefore, using longer RF segments for angular compounding may not be an optimum choice because of the subsequent reduction in the spatial resolution. The optimum length of the RF segment has to be determined by computing the SNR improvement from the correlation coefficient of the parametric estimate vs. insonification angle curves and the corresponding spatial resolution reduction from the area that the RF segment sweeps during angular compounding. In this paper, we derived only the correlation coefficient of RF segments vs. the insonification angle. For different parametric imaging methods, the calculation of the parameter of interest from the RF data segment will differ. Therefore, each parametric modality needs to be studied individually to optimize the angular compounding approach.

Signal decorrelation from the same spatial location has a special property in that it is independent of the insonifi-

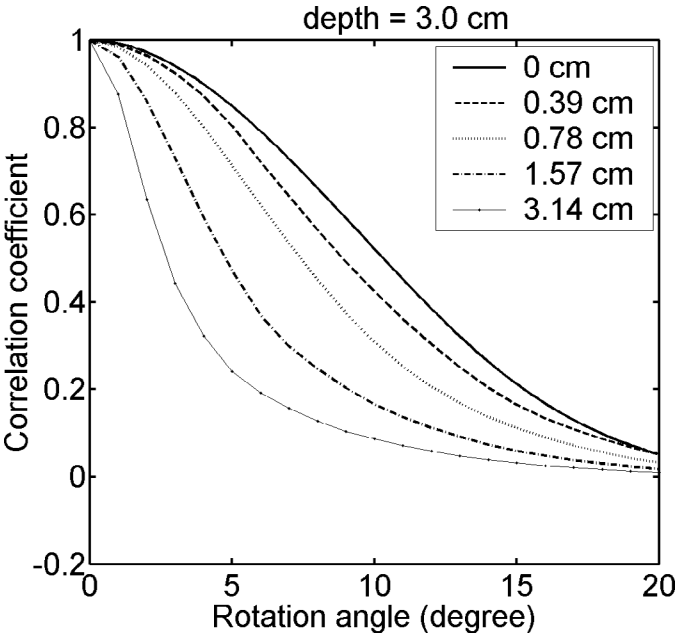

Fig. 6. Theoretical demonstration of decorrelation vs. insonification angle for different RF data segment lengths.

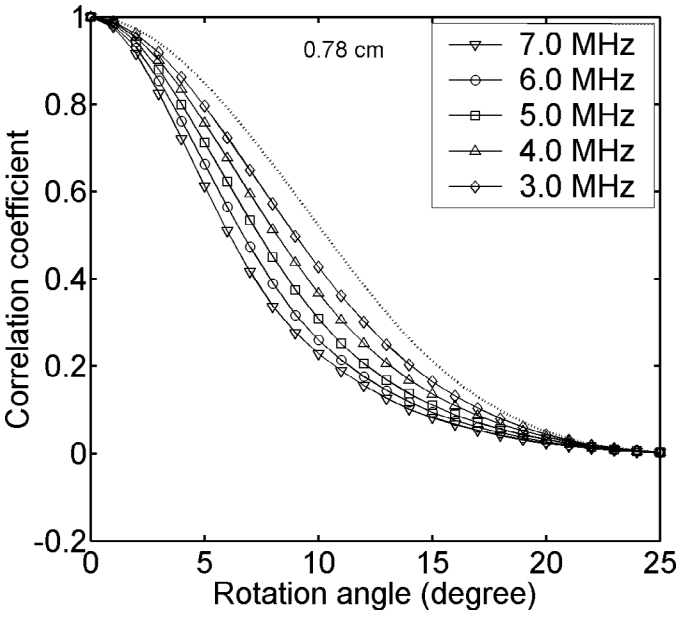

Fig. 7. RF signal segment correlation coefficient vs. beam angle for different insonification frequencies. The dotted line is the correlation coefficient of the RF signal obtained from the same spatial location.

cation frequency. Although an increase in frequency would result in more rapid phase changes with small changes in insonification angle, the concomitant narrower beam would restrict the scatterers contributing to the ultrasound signal at any transducer angle closer to the rotation center. These two opposite effects cancel, making the result insensitive to frequency. However, when we consider the decorrelation of two finite-sized RF data segments, the decorrelation effects do increase with ultrasound frequency. Fig. 7 plots the expected decorrelation during rotation of a RF segment of length 0.78 cm for different frequencies. The RF segment was assumed to be at a 3.0-cm depth in the medium, and the aperture of the transducer was taken to be 1.5 cm. As illustrated in the figure, the higher the insonification frequency, the faster the decorrelation of RF signal pairs. The explanation for this behavior is that the major contribution of decorrelation of the RF segment comes from the signal decorrelation at both ends of the RF segment, for which relative scatterer positions change most rapidly with small changes in beam view directions. At these locations, the more restricted lateral extent of the higher frequency beams does not lessen the decorrelation with angle, as it does when scatterer positions are restricted to those closer to the center of rotation. The RF segment correlation curve will approach the correlation of signals from the same spatial location, illustrated in the dotted curve in Fig. 7, as the insonification frequency decreases. This is due to the concomitant increase in the beam width that negates the larger amount of separation caused by rotation. [$|p'(x-a/2)\|p'(x+a/2)|$ in (19) can be approximated as $|p'(x)\|p'(x)|$; thus (19) reduces to (14)].

Similar behavior is seen when the aperture of the transducer is changed. Fig. 8 plots theoretical correlation curves for different transducer apertures. The horizontal axis is the translation b, as a fraction of the aperture size. The RF segment studied here is again centered at a 3.0-cm depth, and the length is 0.78 cm. The insonification frequency used is 5 MHz. For the correlation of signals obtained with the aperture translated and steered to view the same spatial location, the curve is the same for different aperture sizes in terms of translation as a fraction of aperture size. We plotted it as the dotted curve in Fig. 8. For the correlation of finite-sized RF signal segments at different insonification angles, only a very small aperture, such as the 5-mm aperture shown in the figure, which produces a wide beam, has correlation curves that approximate the dotted curve. For larger apertures, the correlation curve falls off quickly with angle because of the narrower beam. The analysis is similar to that described in the previous paragraph.

VI. Conclusions

We have derived a theoretical expression for the decorrelation of ultrasound RF echo signals as the insonification angle changes. This work is based on previous theoretical results presented by Wagner *et al.* [15], where the analysis was restricted to a target at a fixed depth. We have refined their expression by avoiding most approximations used. Under certain approximations, a closed-form analytical expression can be derived. However, for parametric imaging we require a theoretical expression that takes into account both the insonification angle and the target locations imaged. The theoretical expressions obtained under these conditions have to rely on numerical solutions with and without the simplifying approximations.

The theoretical prediction (23) matches computer simulations very well. This theory is useful for compound-

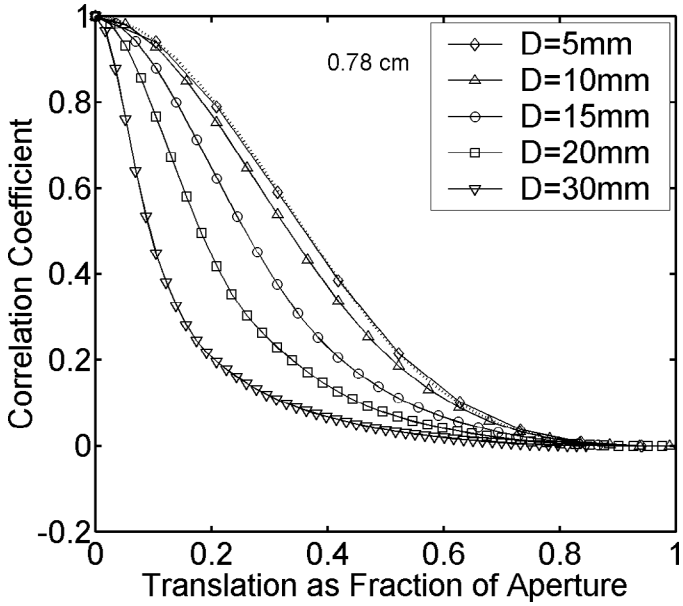

Fig. 8. Theoretical RF signal segment correlation coefficient values for different transducer aperture sizes (D). The dotted line is the correlation coefficient obtained where the RF signal is obtained from the same spatial location.

ing during parametric imaging, where the parameters are calculated from a RF echo signal segment. The theoretical prediction can help in finding optimum compounding schemes for parametric imaging. However, the relationship between the correlation between two RF signal segments and the ensuing correlation between parameters estimated from these segments must also be determined. The relationship may be different for different parametric imaging modalities, reflecting the effects of different signal processing schemes. In the light of this theoretical framework, we have studied the scatterer size imaging [35] and attenuation imaging [36] and found good agreement.

References

[1] J. A. Zagzebski, Z. F. Lu, and L. X. Yao, "Quantitative ultrasound imaging: In vivo results in normal liver," *Ultrason. Imag.*, vol. 15, pp. 335–351, 1993.

[2] Z. F. Lu, J. A. Zagzebski, R. T. O'Brien, and H. Steinberg, "Ultrasound attenuation and backscatter in the liver during prednisone administration," *Ultrasound Med. Biol.*, vol. 23, pp. 1–8, 1997.

[3] F. L. Lizzi, E. J. Feleppa, M. Astor, and A. Kalisz, "Statistics of ultrasonic spectral parameters for prostate and liver examinations," *IEEE Trans. Ultrason., Ferroelect., Freq. Contr.*, vol. 44, pp. 935–942, 1997.

[4] M. F. Insana and T. J. Hall, "Parametric ultrasound imaging from backscatter coefficient measurements: Image formation and interpretation," *Ultrason. Imag.*, vol. 12, pp. 245–267, 1990.

[5] M. F. Insana and T. J. Hall, "A method for characterizing soft tissue microstructure using parametric ultrasound imaging," *Prog. Clin. Biol. Res.*, vol. 363, pp. 241–256, 1991.

[6] M. F. Insana, T. J. Hall, J. G. Wood, and Z. Y. Yan, "Renal ultrasound using parametric imaging techniques to detect changes in microstructure and function," *Invest. Radiol.*, vol. 28, pp. 720–725, 1993.

[7] E. Walach, A. Shmulewitz, Y. Itzchak, and Z. Heyman, "Local tissue attenuation images based on pulse-echo ultrasound scans," *IEEE Trans. Biomed. Eng.*, vol. 36, pp. 211–221, 1989.

[8] B. S. Knipp, J. A. Zagzebski, T. A. Wilson, F. Dong, and E. L. Madsen, "Attenuation and backscatter estimation using video signal analysis applied to B-mode images," *Ultrason. Imag.*, vol. 19, pp. 221–233, 1997.

[9] M. O'Donnell, A. R. Skovoroda, B. M. Shapo, and S. Y. Emelianov, "Internal displacement and strain imaging using ultrasonic speckle tracking," *IEEE Trans. Ultrason., Ferroelect., Freq. Contr.*, vol. 41, pp. 314–325, 1994.

[10] J. Ophir, I. Cespedes, H. Ponnekanti, Y. Yazdi, and X. Li, "Elastography: A quantitative method for imaging the elasticity of biological tissues," *Ultrason. Imag.*, vol. 13, pp. 111–134, 1991.

[11] K. J. Parker, S. R. Huang, R. A. Musulin, and R. M. Lerner, "Tissue response to mechanical vibrations for 'sonoelasticity imaging'," *Ultrasound Med. Biol.*, vol. 16, pp. 241–246, 1990.

[12] S. L. Bridal, B. Beyssen, P. Fornes, P. Julia, and G. Berger, "Multiparametric attenuation and backscatter images for characterization of carotid plaque," *Ultrason. Imag.*, vol. 22, pp. 20–34, 2000.

[13] S. L. Bridal, P. Fornes, P. Bruneval, and G. Berger, "Parametric (integrated backscatter and attenuation) images constructed using backscattered radio frequency signals (25–56 MHz) from human aortae in vitro," *Ultrasound Med. Biol.*, vol. 23, pp. 215–229, 1997.

[14] R. F. Wagner, S. W. Smith, J. M. Sandrik, and H. Lopez, "Statistics of speckle in ultrasound B-scans," *IEEE Trans. Sonics Ultrason.*, vol. 30, pp. 156–163, 1983.

[15] R. F. Wagner, M. F. Insana, and S. W. Smith, "Fundamental correlation lengths of coherent speckle in medical ultrasonic images," *IEEE Trans. Ultrason., Ferroelect., Freq. Contr.*, vol. 35, pp. 34–44, 1988.

[16] A. Gerig, J. Zagzebski, and T. Varghese, "Statistics of ultrasonic scatterer size estimation with a reference phantom," *J. Acoust. Soc. Amer.*, vol. 113, pp. 3430–3437, 2003.

[17] G. E. Trahey, S. W. Smith, and O. T. von Ramm, "Speckle pattern correlation with lateral aperture translation: Experimental results and implications for spatial compounding," *IEEE Trans. Ultrason., Ferroelect., Freq. Contr.*, vol. 33, pp. 257–264, 1986.

[18] G. E. Trahey, J. W. Allison, S. W. Smith, and O. T. von Ramm, "A quantitative approach to speckle reduction via frequency compounding," *Ultrason. Imag.*, vol. 8, pp. 151–164, 1986.

[19] H. E. Melton and P. A. Magnin, "A-mode speckle reduction with compound frequencies and compound bandwidths," *Ultrason. Imag.*, vol. 6, pp. 159–173, 1984.

[20] R. Entrekin and H. E. Melton, "Real-time speckle reduction in B-mode images," *IEEE Trans. Ultrason., Ferroelect., Freq. Contr.*, vol. 27, p. 146, 1980.

[21] R. Entrekin, P. Jakson, J. R. Jago, and B. A. Porter, "Real time spatial compound imaging in breast ultrasound: Technology and early clinical experience," *Medicamundi*, vol. 43, pp. 35–43, 1999.

[22] U. Techavipoo, Q. Chen, T. Varghese, J. A. Zagzebski, and E. L. Madsen, "Noise reduction using angular compounding for elastography," *IEEE Trans. Ultrason., Ferroelect., Freq. Contr.*, vol. 51, pp. 510–520, 2004.

[23] U. Techavipoo, Q. Chen, T. Varghese, and J. A. Zagzebski, "Estimation of displacement vectors and strain tensors in elastography using angular insonifications," *IEEE Trans. Med. Imag.*, vol. 23, pp. 1479–1489, 2004, submitted for publication.

[24] A. Gerig, T. Varghese, and J. A. Zagzebski, "Improved parametric imaging of scatterer size estimates using angular compounding," *IEEE Trans. Ultrason., Ferroelect., Freq. Contr.*, vol. 51, pp. 708–715, 2004.

[25] H. Tu, T. Varghese, E. L. Madsen, Q. Chen, and J. A. Zagzebski, "Ultrasound attenuation imaging using compound acquisition and processing," *Ultrason. Imag.*, vol. 25, pp. 245–261, 2003.

[26] S. W. Smith, R. F. Wagner, J. M. Sandrik, and H. Lopez, "Low contrast detectability and contrast/detail analysis in medical ultrasound," *IEEE Trans. Sonics Ultrason.*, vol. 30, pp. 164–173, 1983.

[27] S. M. Gehlbach, "Pulse reflection imaging and acoustic speckle," Ph.D. dissertation, Stanford University, Stanford, CA, 1983.

[28] C. B. Burckhardt, "Speckle in ultrasound B-mode scans," *IEEE Trans. Sonics Ultrason.*, vol. 25, pp. 1–6, 1978.

[29] M. O'Donnell and S. D. Silverstein, "Optimum displacement for compound image generation in medical ultrasound," *IEEE Trans. Ultrason., Ferroelect., Freq. Contr.*, vol. 35, pp. 470–476, 1988.
[30] W. F. Walker and G. E. Trahey, "The application of k-space in pulse and echo ultrasound," *IEEE Trans. Ultrason., Ferroelect., Freq. Contr.*, vol. 45, pp. 541–558, 1998.
[31] R. J. Zemp, C. K. Abbey, and M. F. Insana, "Linear system models for ultrasonic imaging: Application to signal statistics," *IEEE Trans. Ultrason., Ferroelect., Freq. Contr.*, vol. 50, pp. 642–654, 2003.
[32] F. L. Lizzi, M. Astor, E. Feleppa, M. C. Shao, and A. Kalisz, "Statistical frame work for ultrasonic spectral parameter imaging," *Ultrasound Med. Biol.*, vol. 23, pp. 1371–1382, 1997.
[33] Y. Li and J. Zagzebski, "Frequency domain model for generating B-mode images with array transducers," *IEEE Trans. Ultrason., Ferroelect., Freq. Contr.*, vol. 46, pp. 690–699, 1999.
[34] J. J. Faran, "Sound scattering by solid cylinders and spheres," Harvard University, Cambridge, Massachusetts, Technical Memorandum 22, March 15, 1951.
[35] A. Gerig, Q. Chen, and J. A. Zagzebski, "Correlation of ultrasonic scatterer size estimates for the statistical analysis and optimization of angular compounding," *J. Acoust. Soc. Amer.*, vol. 116, pp. 1832–1841, 2004.
[36] H. Tu, J. A. Zagzebski, A. Gerig, Q. Chen, E. L. Madsen, and T. J. Hall, "Optimization of angular and frequency compounding in ultrasonic attenuation estimation," *J. Acoust. Soc. Amer.*, vol. 117, pp. 3307–3318, 2005, submitted for publication.

Quan Chen (S'03) was born in Xinhua, China, in 1975. He received his B.S. degree in Physics from Nanjing University, China, in 1996. He spent two years in the Master's program in Physics, Southeast University, China, before coming to the United States in 1998. He earned a M.S. degree and a Ph.D. degree in medical physics in 2004 at the University of Wisconsin-Madison. He is currently employed by Tomotherapy Inc., Madison, WI to develop image processing techniques for image-guided radiation therapy (IGRT).

His research interests include computer modeling in ultrasound, parametric imaging (elastography, scatterer size, and attenuation) and computer vision in medical imaging (including segmentation and deformable registration in ultrasound and CT images).

Anthony L. Gerig (S'02–M'04) was born on December 30, 1975 in Decatur, IN. He received the B.S. degree in physics and mathematics from Taylor University, Upland, IN in 1998, and the M.A. and Ph.D. degrees in physics from the University of Wisconsin-Madison in 2002 and 2004 respectively. He is currently a postdoctoral scholar at the Penn State Applied Research Lab. Research interests include statistical signal processing, acoustic scattering and propagation, and ultrasonic beamforming and tissue characterization. Dr. Gerig is a member of the IEEE and the Acoustical Society of America.

Udomchai Techavipoo (S'01–M'05) was born in Bangkok, Thailand, on September 16, 1973. He received the B.Eng.E.E. degree from Kasetsart University, Bangkok, Thailand, in 1994. In 1997, he received a scholarship from Anandamahidol Foundation, Thailand, to pursue graduate studies at the College of Engineering, the University of Michigan, Ann Arbor, and received the M.S.E.E. degree in 1999. He received a Ph.D. degree in electrical engineering at the University of Wisconsin-Madison, in 2004. His thesis topic is ultrasound elastography and non-invasive temperature estimation. He is currently a research fellow at the Thomas Jefferson University MRI physics lab. His research interests include signal and image processing applications in medical imaging.

James Zagzebski (A'89) was born in Steven Points, WI in 1944. He received the B.S. degree in physics from St. Mary's College, Winona, MN, and the M.S. degree in physics and the Ph.D. degree in radiological sciences from the University of Wisconsin, Madison. He is Professor of medical physics and of radiology and human oncology at the University of Wisconsin.

His research interests include ultrasound imaging and tissue characterization, flow detection and visualization using ultrasound, and technological assessment of imaging devices. Dr. Zagzebski's professional affiliations include the IEEE, the American Institute of Ultrasound in Medicine, and the American Association of Physicists in Medicine.

Tomy Varghese (S'92–M'95–SM'00) received the B.E. degree in Instrumentation Technology from SJCE, University of Mysore, India in 1988, and the M.S. and Ph.D. degrees in electrical engineering from the University of Kentucky in 1992 and 1995, respectively. From 1988 to 1990 he was employed as an Engineer in Wipro Information Technology Ltd. India. From 1995 to 2000, he was a post-doctoral research associate at the Ultrasonics laboratory, Department of Radiology, University of Texas Medical School, Houston. He is currently an Assistant Professor in the Department of Medical Physics at the University of Wisconsin-Madison. His current research interests include elastography, ultrasound imaging, ultrasonic tissue characterization, detection and estimation theory, statistical pattern recognition and signal and image processing applications in medical imaging. Dr. Varghese is a member of the IEEE, the American Institute of Ultrasound in Medicine (AIUM), the American Association of Physicists in Medicine (AAPM) and Eta Kappa Nu.